OPTIMAL AIRFOIL DESIGN AND WING ANALYSIS FOR SOLAR-POWERED HIGH ALTITUDE PLATFORM STATION

by

Mohammad Sakib HASAN[a*], Jelena M. SVORCAN[a], Aleksandar M. SIMONOVIĆ[a], Nikola S. MIRKOV[b], and Olivera P. KOSTIĆ[a]

[a] Faculty of Mechanical Engineering, University of Belgrade, Belgrade, Serbia
[b] Vinča Institute of Nuclear Sciences, National Institute of the Republic of Serbia, University of Belgrade, Belgrade, Serbia

Original scientific paper
https://doi.org/10.2298/TSCI210419241S

The ability of flying continuously over prolonged periods of time has become target of numerous research studies performed in recent years in both the fields of civil aviation and unmanned drones. High altitude platform stations are aircrafts that can operate for an extended period of time at altitudes 17 km above sea level and higher. The aim of this paper is to design and optimize a wing for such platforms and computationally investigate its aerodynamic performance. For that purpose, two-objective genetic algorithm, class shape transformation and panel method were combined and used to define different airfoils with the highest lift-to-drag ratio and maximal lift coefficient. Once the most suitable airfoil was chosen, polyhedral half-wing was modeled and its aerodynamic performances were estimated using the CFD approach. Flow simulations of transitional flow at various angles-of-attack were realized in ANSYS FLUENT and various quantitative and qualitative results are presented, such as aerodynamic coefficient curves and flow visualizations. In the end, daily mission of the aircraft is simulated and its energy requirement is estimated. In order to be able to cruise above Serbia in July, an aircraft weighing 150 kg must accumulate 17 kWh of solar energy per day.

Key words*: optimization, wing design, CST parameterization, XFOIL, genetic algorithm, CFD*

Introduction

High altitude pseudo-satellites (HAPS) are a new concept in the development of flying vehicles that has been referred to by several different names over the years, including *high altitude powered platform*, *high altitude aeronautical platform*, *high altitude airship*, *stratospheric platform*, *stratospheric airship*, *high altitude long endurance* (HALE), and *atmospheric satellite*. These are aircrafts which operate at stratospheric altitudes (17-25 km) and provide services like environmental monitoring, remote sensing, weather forecasting and telecommunications. Several types of high altitude solar unmanned aerial vehicles (UAV) have already been developed. Under NASA environmental research aircraft and sensor technology program, AeroVironment, Inc. developed solar-powered drones called Pathfinder, Centurion, and Helios at the end of 1993. Recently, Airbus has flown again the Zephyr S which they bought from QinetiQ in 2013. and achieved a flight endurance record of 14^{+} days without refueling. In less than two years, BAE SYSTEM and Prismatic Ltd. collaborated to design the PHASA-35, a

* Corresponding author, e-mail: sakibhasan89@yahoo.com

persistent high altitude solar aircraft (PHASA) which completed its maiden flight in 2020. The PHASA-35 has the ability to fly non-stop for a year. In order to achieve target endurance which is not easy to acquire, solar-powered electric platforms are used. Photovoltaic modules can be used to collect solar energy during the day, with one part being used to power the propulsion unit and onboard instruments immediately and the other being stored for later use [1-7].

One of the most crucial stages in the aircraft design process is optimization. It improves the process' efficiency without increasing the cost. Goraj and Spalding [8] provide an overview of the civil HALE UAV design activity, stating that improving aerodynamic efficiency and optimizing aircraft structures could reduce operational costs. In recent years, a significant amount of research has been conducted in the field of airfoil shape optimization, as this process helps to improve airfoil's performance as well as the performance of the whole aircraft which is more than beneficial since power consumption can be significant. Since endurance (flight duration) and range (path length) are very important performance characteristics of HAPS UAV, their optimization can lead to longer endurance and range as well as decreased power consumption. A lot of studies try to optimize geometric parameters of airfoils to find a better glide ratio, hence better endurance, but it requires additional effort. Many examples of their parameterization and optimization can be found in [9-17]. Park *et al*. [9] combined the multi-objective optimization technology with CFD to optimize the shape of an airfoil with a high aspect ratio for a long-range UAV. Gardner *et al*. [10] observed results from 400 cases and came to a conclusion that ProfoilGA and BezierGA are both reliable in finding an airfoil with a 14% reduction in drag. Leloudas et *al*. [11] used a differential evolution algorithm to perform a constrained (area-preserving) airfoil optimization, with XFOIL [18] estimating the aerodynamic performances of each considered airfoil. Mukesh *et al*. [12], starting with NACA 2411 airfoil, an aerodynamic shape optimization process is formulated and solved and the optimized airfoil is validated through experimental process, while the results by genetic algorithm (GA) for the optimized airfoil are found to be reasonably close to the results obtained from wind tunnel measurements. Viola *et al*. [13] used an evolutionary optimization algorithm to help them define an optimal four-digit NACA airfoil using *transition SST* turbulence model [19]. All of these examples resulted in new streamlined contours with the primary goal of increasing the 3-D body's aerodynamic efficiency.

In this paper, class-shape transformation (CST) parameterization [20] was used for the development of a new airfoil that is parameterized by 6 input parameters. We used a relatively recent two-objective GA optimization [21, 22] in conjunction with the freely available XFOIL [18] to estimate aerodynamic coefficients of low resolution airfoils. Adopted computational model was validated through comparison of the obtained numerical data with the corresponding experimental results from a well known airfoil FX 63-137 [23]. Afterwards, a wing was designed by using the optimal airfoil which had the highest glide ratio and an estimation of its aerodynamic performance was performed by CFD methods in ANSYS FLUENT [24], by closing the governing flow equations by *transition SST* turbulence model. In the end, daily mission of the aircraft is simulated, its energy requirement is estimated and the most important conclusions are provided.

Airfoil optimization

The development of future HALE/HAPS UAV relies heavily on the design of its main lifting surface such as wing. Aerodynamic shape optimization, also known as aerodynamic design optimization, is the method of modifying the shape of a body (such as an airfoil or wing) to improve its performance. Here, the goal is to create efficient and aerodynamically sound optimal airfoil by using CST parameterization and GA.

The CST parameterization

The use of evolutionary algorithms for airfoil optimization has become common in the design of aircraft wings and propeller blades. Airfoil shapes are typically created as compound curves or splines which must be parameterized in a simple and smooth way in order to perform satisfactory optimization. Although a variety of parameterization methods are in use, the CST introduced by Boeing employee Kulfan [20] is widely applied because of its simplicity, robustness, and its ability to be generalized into various possible shapes of aerodynamic bodies.

In short, the method is based on Bezier curves and consists of two functions: a class function that generalizes different 2-D airfoils and 3-D body geometries and an analytic shape function which allows an easy control of the critical design parameters (leading edge radius, trailing edge boat tail angle*, etc.*) of the airfoil. The general equation that represents the typical airfoil can be written:

$$\zeta(\psi) = \sqrt{\psi}(1-\psi)\sum_{i=0}^{N} A_i \psi^i + \psi\zeta_T \tag{1}$$

where $\psi = x/c$, $\zeta = z/c$ and $\zeta_T = \Delta\zeta_{TE}/c$.

The terms $\psi^{1/2}$ and $(1 - \psi)$ insure round nose and a sharp trailing edge, respectively, $\psi\zeta_T$ allows to control the thickness of the trailing edge and represents a general feature that defines the distinct geometry between the round nose and the sharp aft end. The term $\psi^{1/2}(1 - \psi)$ is the class-function and it can be defined:

$$C_{N_2}^{N_1}(\psi) = \psi^{N_1}(1-\psi)^{N_2} \tag{2}$$

The values N_1 and N_2 define whether the airfoil nose and tail are round or pinpointed. If N_1 is 0.5, airfoil nose shape is round, whereas its end is pinpointed if the value of N_2 is 1. The shape function is obtained by a Bernstein polynomial, eq. (3), and a set of curvature coefficients for a given airfoil that scale the corresponding binomial coefficients:

$$S(\psi, i) = K_i^N \psi^i (1-\psi)^{N-i} \tag{3}$$

The following are some of the specially convenient and efficient properties of using Bernstein polynomials to describe an airfoil:

- The entire design space of geometrically smooth airfoils is captured using this airfoil representation technique.
- The unit form factor airfoil can be used to build any airfoil in the design space.
- As a consequence, every airfoil in the design space can be derived from any other airfoil.

The degree of polynomials in this case was $N = 2$, which implies that each pressure and suction side of the airfoil was described by three coefficients of negative and positive values, respectively, resulting in six input parameters in total. The ranges of possible absolute values of the three input coefficients are limited, thus implicitly dictating the minimal and maximal relative thicknesses of the airfoil to 6% and 35%, respectively. This consideration is included to ascertain geometrically viable designs that are, at the same time, structurally reliable. The defined shape of the airfoil could then be described by a large number of pairs of points (*e.g.*, 100) where *x*-co-ordinates were obtained by cosine distribution better present the leading and trailing edges, and *z*-co-ordinates were computed as described previously.

Genetic algorithm

The GA are adaptive optimization methods derived from the genetic process of biological organisms. They mainly simulate processes which are essential for evolution. These algorithms prefer individuals that are more successful in surviving (*i.e.* individuals capable of

providing solution a given problem). The most successful individuals attract other mates and have a relatively large number of offspring. Each individual is scored by a fitness function that quantifies how effective it is at solving the problem. To prevent the optimization procedure from converging to a local minimum or a sub-optimal solution, various selection methods are used. Uniforms, roulette, tournaments, *etc.* are among the most popular [21].

With respect to the number of input parameters, the population numbered 400 entities. More than 1000 generations were formed, resulting in nearly 400000 individual computations.

As previously mentioned, each considered entity was defined by six coefficients that served to define the shape of the airfoil whose aerodynamic characteristics at 0.20 MRe were computed by XFOIL [18].

In order to perform multi-objective optimization, two distinct objective functions whose maximal values are sought were defined, best glide ratio and best maximal lift coefficient:

$$\max\left(\frac{C_L}{C_D}\right) \wedge \max\left(C_{L,\max}\right) \tag{4}$$

A more comprehensive overview of GA is given in [21, 22].

Computational model validation

In order to ascertain the validity of adopted computational approach as well as the usefulness of obtained optimized airfoils, in the beginning, the numerical results obtained by XFOIL [18] (a relatively simple but very useful and powerful solver, particularly applicable to low Reynolds numbers airfoils, based on panel methods and enhanced by various semi-empirical corrections capable to sufficiently accurately describe viscous flow in the vicinity of walls, laminar separation bubble, laminar-to-turbulent transition and other viscous effects dominating at low Reynolds numbers) were compared to the corresponding experimental data acquired in wind tunnel measurements on the airfoil FX 63-137 (that is designed for small speeds and Reynolds numbers and is illustrated in fig. 1). A detailed description of performed experimental investigation can be found in [23].

Figure 1. Airfoil FX 63-137

Figure 2 presents the computed and measured lift and drag coefficient curves of the airfoil FX 63-137. As expected, due to the high airfoil curvature, computed results are somewhat overrated. Computed lift gradient is higher, while the computed drag coefficient at smaller

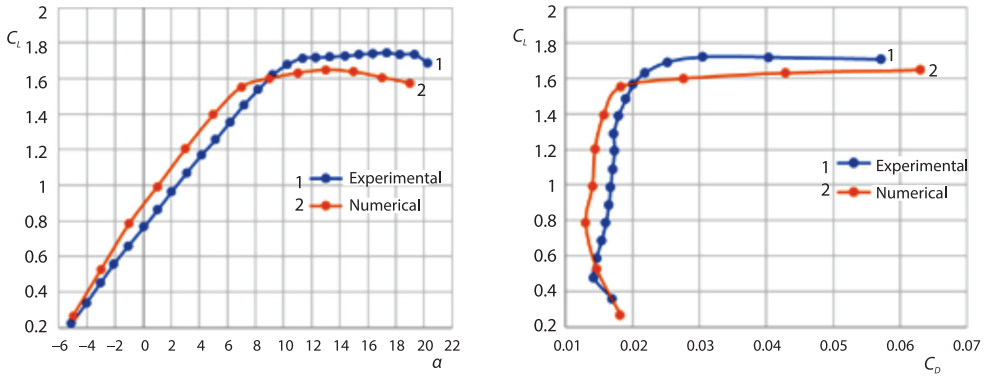

Figure 2. Lift and drag coefficient curves of airfoil FX 63-137, Re = 200.000

angles-of-attack (AoA) is lower than measured. However, the trend of both curves is well captured and the overall agreement is satisfactory implying that XFOIL can be used in preliminary optimization studies as long as the researcher keeps in mind that not all geometric features or viscous effects could be adequately simulated. Additionally, at high AoA, the estimations of maximal lift coefficient and critical AoA are slightly underrated, while the total drag coefficient is a little overestimated. Both of these assertions imply that the calculated glide ratio remains on the safety side at high AoA.

Optimized 2-D airfoils

Figure 3 illustrates the obtained Pareto front, together with the values of goal functions of the last generation. It can be concluded that, by conducting two-criteria optimization, superb airfoil aerodynamic performances seem achievable. Maximal values of lift-to-drag (or glide) ratio C_L/C_D are nearly 88, while maximal lift coefficient $C_{L,\max}$ amounts to 1.67. Of course, both goals cannot be accomplished at the same time, and it is necessary to compromise or choose one of the two considered. In the case of HAPS, greater lift-to-drag implies longer endurance and smaller height loss during nighttime and can therefore, be chosen as the main norm for selecting an optimal airfoil from the generated Pareto set.

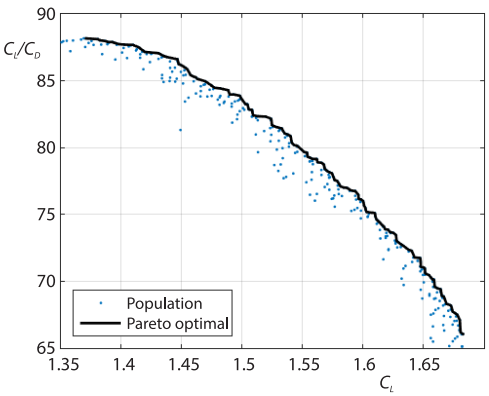

Figure 3. Obtained Pareto front

In order to better comprehend the characteristics of airfoils forming the Pareto set, three airfoils are chosen for comparative analysis. Airfoil-1 has the best glide ratio, Airfoil-3 has the highest maximal lift coefficient, while Airfoil-2 is somewhere in between. Their geometric properties (maximal relative thickness $(t/l)_{\max}$ and its relative position, maximal relative curvature $(c/l)_{\max}$ and its relative position) are listed in tab. 1, whereas their shape and aerodynamic characteristics are illustrated in figs. 4 and 5.

Table 1. Geometric properties of chosen airfoils

	$(t/l)_{\max}$ [%]	at x/l [%]	$(c/l)_{\max}$ [%]	at x/l [%]
Airfoil-1	12.36	34.53	4.87	46.95
Airfoil-2	14.00	31.53	5.55	43.74
Airfoil-3	15.97	28.73	6.59	37.54
FX 63-137	13.71	30.83	5.97	53.35

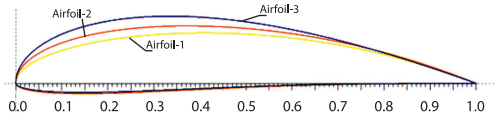

Figure 4. Contours of chosen airfoils

Interestingly, the airfoils mainly differ in the suction contour (inducing differences in thickness and curvature), while their lower surface is almost the same. As previously mentioned, Airfoil-3 has the highest maximal lift coefficient ($C_{L,\max}$ = 1.65), while the respective values for Airfoil-2 and Airfoil-1 are 1.55 and 1.45. However, all three airfoils behave favorably near stall since there are neither sudden changes nor significant lift losses at high AoA. At medium AoA ($3° \leq \alpha \leq 8°$), drag coefficients of all three airfoils are in the range [0.013, 0.020] which is acceptable, while sudden drag rise happens at $\alpha > 10°$. Estimated glide ratios of airfoils 1-3 for $3° \leq \alpha \leq 8°$ are approximately 85 (which is very satisfactory), 79, and 70, respectively.

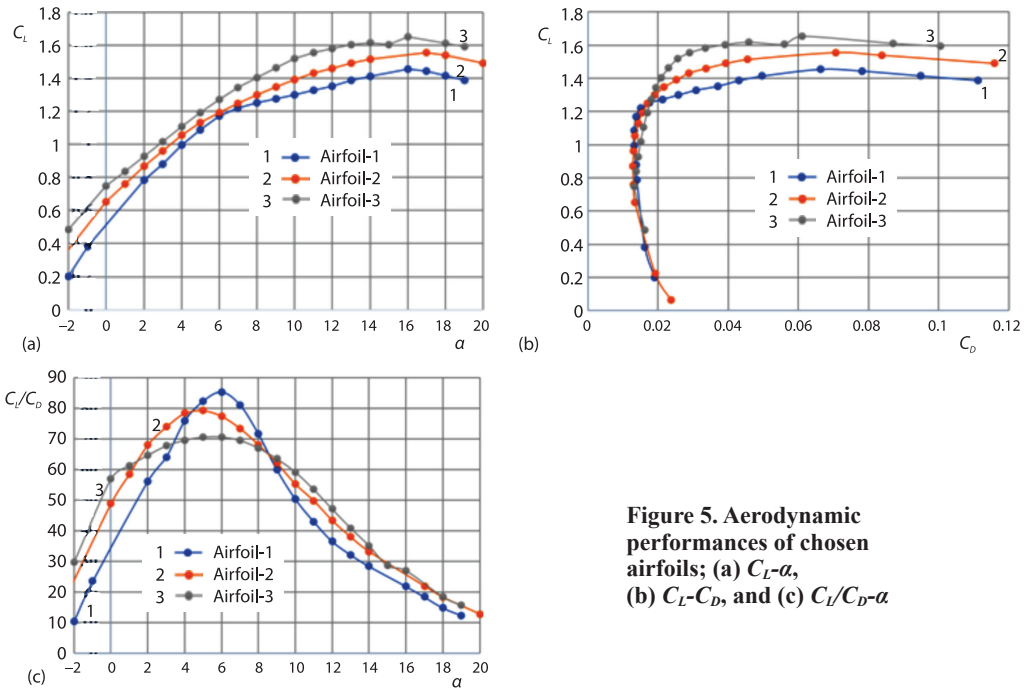

Figure 5. Aerodynamic performances of chosen airfoils; (a) C_L-α, (b) C_L-C_D, and (c) C_L/C_D-α

Although presented results are obtained by simplified 2-D analyses, and will certainly diminish when applied to 3-D wing, they are promising and point to the direction of optimal wing geometry specially developed for HAPS. Here, Airfoil-1 that has the highest glide ratio is chosen for the following wing design and more detailed analysis.

Wing design

The wing configuration is very important in the design stage of UAV. In this study, the intended HAPS take-off mass is 150 kg, and its main lifting surface must generate sufficient lift force to enable steady flight or glide at 20 km altitude. Additionally, the wing should have the highest possible usable area (that can accommodate numerous solar panels) and should be the easiest and most economic to build. All these requests have led to the choice of a high aspect-ratio, two-section wing comprising an inner rectangular and an outer trapezoid part, while one-segmented wing configuration was previously studied in [25]. Furthermore, it is intended that the wing be untwisted since its stalling characteristics can directly be related to the airfoil stalling characteristics, that seem to be very satisfactory, as previously illustrated in fig. 5. At the same time, the manufacturing of an untwisted composite wing, in comparison twisted, is greatly facilitated and can be performed in segments from the same mould. Also, the wing aspect-ratio is sufficiently high to eliminate the unfavorable effects of induced drag (*i.e.* the vortices separating from the wing tips). Most of the solar powered HAPS UAV have polyhedral wings as they are prone to deform (*i.e.* bend) significantly in flight under aerodynamic loads due to their high aspect-ratios and structural elasticity. Here, a wing with dihedral tip is designed and modeled and its performance is studied. Also, to further enhance the span-wise load distribution, the outer wing segment is tapered. Taper ratio close to 0.6, that is recommended for untwisted wings, is used. Small tail surfaces, attached to thin tail booms and positioned

sufficiently behind the wing, are intended for providing static stability. However, since they are much smaller and lighter than the wing and batteries, they are not considered in more detail.

Wing geometry

Half-span of the designed two-segmented wing is $b/2 = 16.55$ m where the first rectangular segment is 11.05 m long and its chord length is 1.50 m, as demonstrated in fig. 6. Wing reference area is approximately 46.5 m^2. In order to cruise at 25 m/s velocity and 20 km altitude, the wing should achieve a lift coefficient close to 1. Taper ratio of the outer, trapezoid segment is 0.6 while its dihedral angle is set to 10.44°.

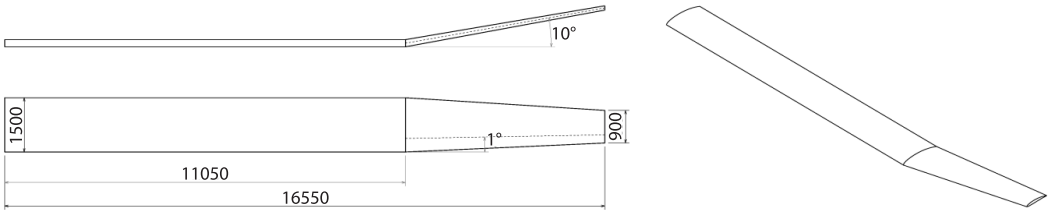

Figure 6. Geometric features of the designed wing

Aerodynamic performance analysis

Modelling, meshing and flow simulations were realized in ANSYS. Computational domain surrounding the half-wing is generated from a quarter-sphere with a radius 2*b*, and a half-cylinder spanning 100 m aft of the wing leading edge. Generated mesh is hybrid unstructured. Inflation of 20 layers with growth rate of 1.2 was used to locally refine the mesh around the wing surface. The root and tip airfoils, as well as the leading and trailing edges of the wing, had different edge sizing functions assigned to them. Eventually, a fine mesh was created with 4651546 elements. Figure 7 shows the domain model and details of the mesh around the wing.

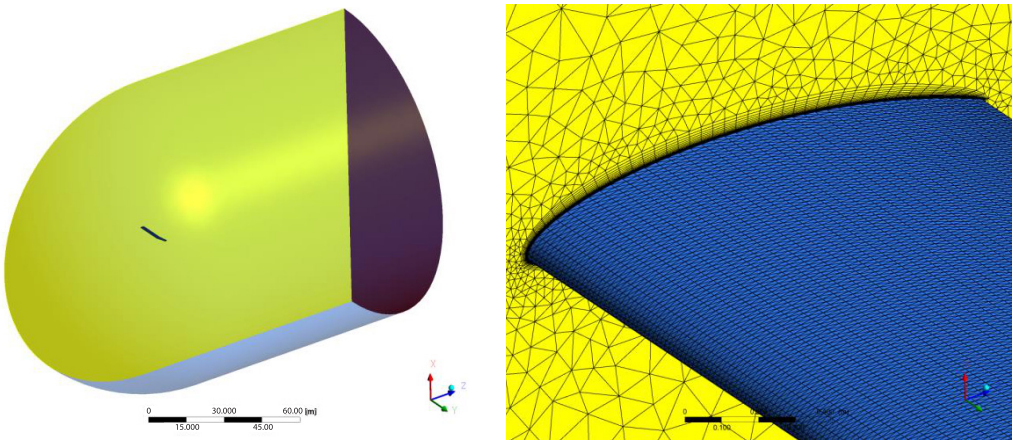

Figure 7. Computational domain and detail of the generated mesh

Wing aerodynamic performances are evaluated using ANSYS FLUENT where mass, momentum, and energy conservation equations are solved by finite volume method [24]. Fluid-flow is considered as 3D and steady while the pressure based solver is used as it is more suitable for incompressible flow.

Physical properties of air and boundary conditions are considered at operating altitude h = 20 km. Simulations were performed for five different AoA while the inlet velocity magnitude was kept at 25 m/s, and zero gauge pressure was assumed at the outlet.

Well proven *transition SST* turbulence model is used for the closure of flow equations [19]. This model has been designed for aerodynamic applications assuming partly laminar flow that transforms to transitional and ultimately turbulent. It is well suited for small speed flows around laminar airfoils. SIMPLEC pressure-velocity coupling scheme was used and the simulations were carried out with spatial discretizations of 2nd order of accuracy.

Figure 8 presents the computed aerodynamic performances of the designed wing. Although maximal glide ratio C_L/C_D is much smaller in comparison the previously obtained airfoil value, its value of nearly 32 is still satisfactory for 3-D geometry. This is mostly caused by the much increased viscous drag, while the wing lift coefficient curve quite resembles its 2-D counterpart. Also, moderate lift loss and steady behavior at higher AoA are preserved which is very important for aircraft safety. Further slight lift-to-drag ratio reduction can be expected when propellers and vertical tail surfaces are added. It can also be observed that the lift coefficient of 0.5 to 1 needed for cruise at heights 15 km and 20 km, respectively, can be achieved for AoA in the range [1°, 6°].

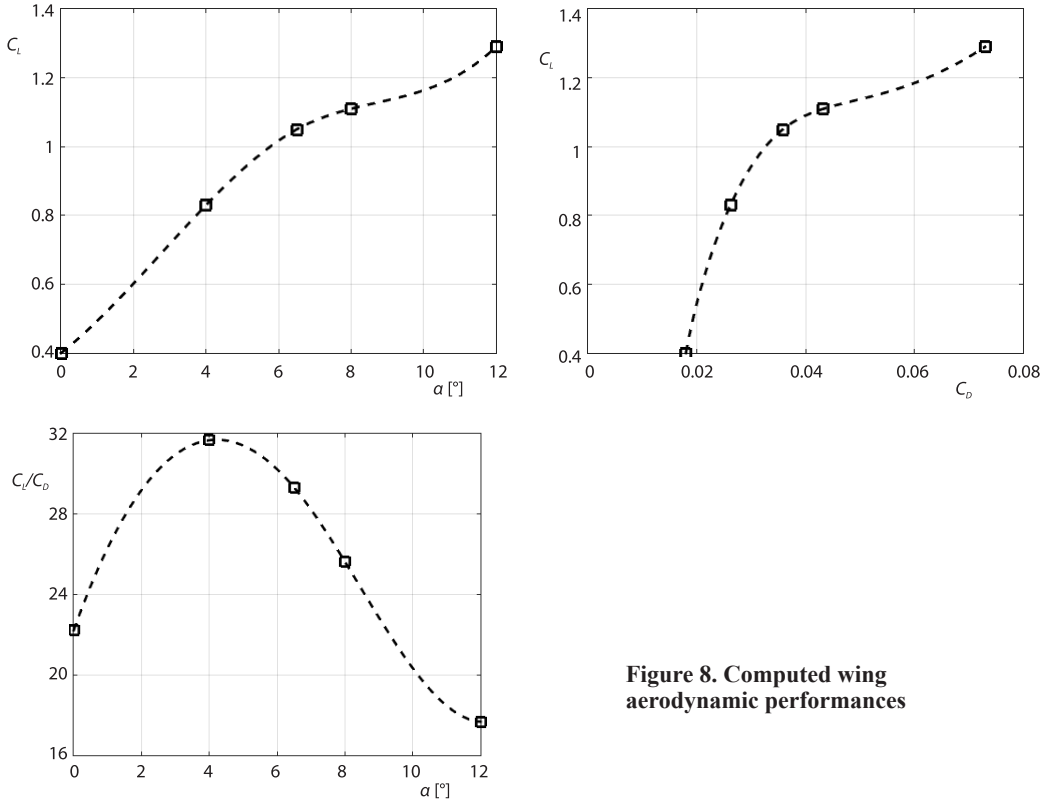

Figure 8. Computed wing aerodynamic performances

Additional flow analysis and visualization can be conducted. Pressure coefficient distributions in four cross-sections (y = 0 m, y = 5 m, y = 10 m, and y = 15 m) demonstrate the favorable aerodynamic distributions in both chord- and span-wise directions. Along the greatest part of the wing (rectangular and for more than half of the trapezoid portion), pressure coeffi-

cient distribution is almost constant as illustrated in fig. 9. Drop in aerodynamic loads (and accompanying losses) appear only in the cross-section whose lateral co-ordinate is y =15 m (closest to the wing tip). Similar conclusions can be drawn if velocity contours in four cross-sections are inspected as presented in fig. 10. Flow is smooth and attached along the greatest part of the wing, and even laminar at the fore half of the suction surface.

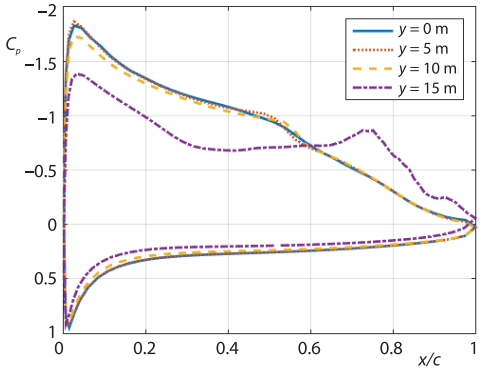

Figure 9. Computed pressure coefficient distributions (*for color image see journal web site*)

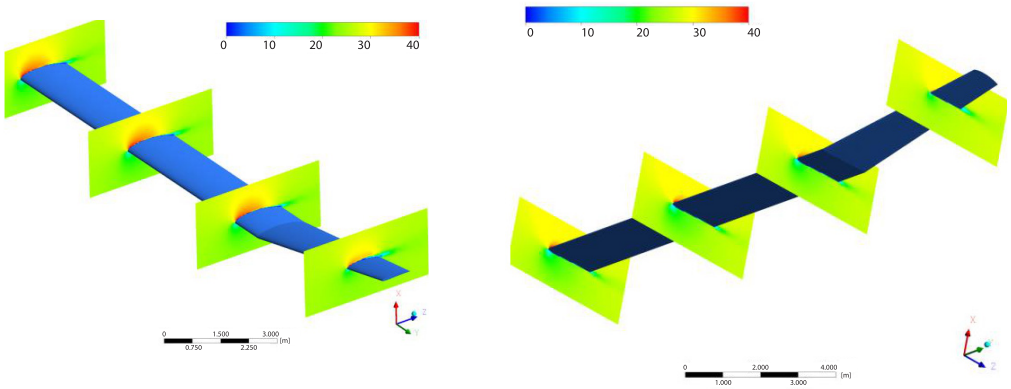

Figure 10. Computed velocity contours

As illustrated in fig. 11, in cruising regime, streamlines follow the wing surface almost till the trailing edge, while vortical structures and uneven flow appear solely near the wing tips thus significantly limiting the induced drag.

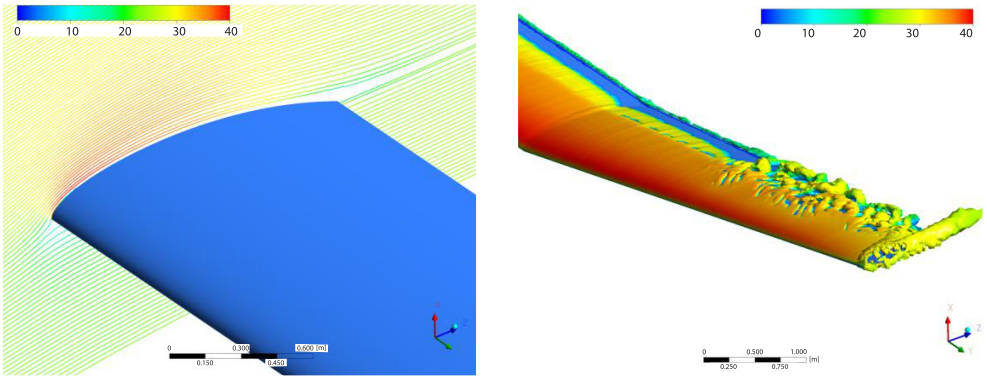

Figure 11. Computed streamlines and vortical structures colored by velocity

Solar power collection, storage and usage

One of the main design requirements of the investigated HAPS is to remain airborne for several months over certain regions, *e.g.* Serbia or Bangladesh, where it could be used to improve global communication or observance capabilities. For that purpose, HAPS propulsion system must incorporate (specially designed) propellers, an example of an optimization study is given in [26], connected to electric motors and a controller. Additionally, it must carry a power collecting and storage system comprising solar panels (distributed along the upper surface of the wing) and batteries. Solar cell dimensioning and performance estimation should be included in the very beginning of the HAPS wing design process, since it directly affects the success of the complete aircraft. It should also be mentioned that the amount of collected power depends on many factors, such as the efficiency of solar cells, geographic location, time of year, weather conditions*, etc.*

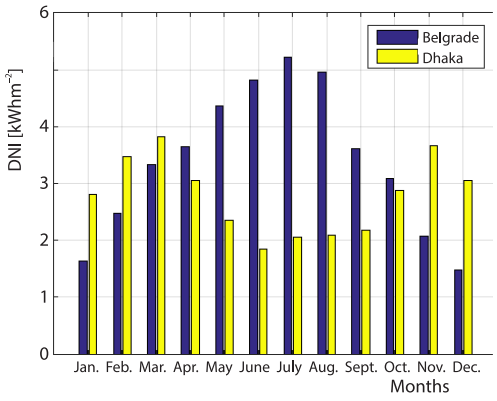

Figure 12. Averaged yearly DNI above Belgrade and Dhaka

Planned HAPS mission is quite demanding. Aircraft weighing 150 kg should first be able to climb to the cruise altitude during daytime (*i.e.* within a time limit of 8 hours). Afterwards, it should be able to repeat the everyday cycles of cruise, descend and climb between the altitudes 20 km and 15 km (during day- and night-time). Therefore, particularly unfavorable working conditions that involve periods of short daylight and/or significantly decreased direct normal solar irradiation (DNI) were not considered here. Instead, summer months were considered for Belgrade, located at approximately 45° northern latitude, while in Dhaka (approximate northern latitude is 24°) the month with the most DNI is March, as illustrated in fig. 12. All irradiance data are freely available at [27].

It is assumed that 75% of the wing suction surface, approximately 35 m^2, is covered by arrays of solar modules. Tiling begins from the root and leading edge and expands towards the trailing edge and wing tips. The remainder of wing area is preserved for control surfaces or not considered due to its small relative thickness. It is also assumed that the aircraft will be able to position itself normal to the oncoming sunlight, by small pitching, rolling or yawing maneuvers, similar to [4], during daytime thus maximizing the collected solar power. Total mass of solar panels of approximately 9 kg can be estimated as the product of their reference area and solar cell density of 0.3 kg/m^2, while the assumed solar cell efficiency is 23%-31% (lower value is for Belgrade, higher for Dhaka, as will be explained in continuation).

Figure 13 presents simulations of a 24 hours flight in optimal working conditions (during a month with the shortest nighttime duration and highest available DNI) for Belgrade and Dhaka, respectively. Collected solar power is denoted by P_{solar}, power required for flight by P_{req}, while their difference ΔP is used to charge (or deplete) the batteries. First task of the power system during daytime is to sustain steady flight at 20 km, power the electric motors and send excess power to batteries. Once the Sun sets, in order to preserve some energy, the aircraft may be allowed to glide to the (minimal) height of 15 km, where it must continue to cruise. This mission segment must be sustained by the power accumulated in batteries during daytime. As the Sun rises anew, solar panels continue to provide energy and charge the batteries, the aircraft

climbs back to the upper cruising height of 20 km, and the whole cycle repeats. Power required for (cruise and) climb is estimated:

$$P_{\text{req}} = \frac{TV_{cr}}{\eta + LV_c} \tag{5}$$

where thrust force, T, equals drag force, D, lift force, L, equals aircraft weight, assumed climb speed is $V_c = 0.83$ m/s (which corresponds to the maximal glide ratio) and propeller efficiency $\eta = 0.8$.

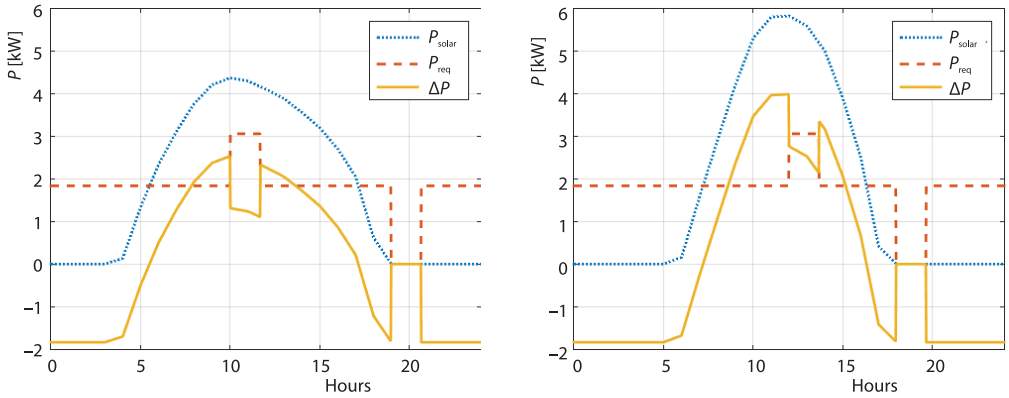

Figure 13. Estimated daily power requirement

The amounts of available and required energy for a single-day flight above Belgrade in July match at nearly 43 kWh (obtained by integrating the power curves per day), out of which approximately 17 kWh must be stored in batteries for nighttime flight. With the assumed specific energy density of batteries of 400 Wh/kg [28], total required mass of batteries reaches nearly 42 kg, which makes up 28% of the total HAPS mass.

Since available solar irradiation levels are significantly lower in Dhaka and the number of daytime hours is lower, the assumed wing design is capable of flight only if solar panels of higher efficiency are assumed. Therefore, with the value of 31%, presented HAPS shall be able to cruise above Bangladesh in March only if energy of 22 kWh per day can be accumulated, *i.e.* with the necessary battery mass of 55 kg corresponding to 37% of total aircraft mass.

Conclusions

Challenges of HALE flight are numerous: low air pressure and density, sub-zero temperatures, low Reynolds number implying accentuated viscosity effects, flight autonomy, need to generate energy for flight, *etc.* This paper provides some solutions to the raised questions of HAPS design. Although many questions remain open, some conclusions and recommendations can be summarized as follows.

- Definition of novel airfoils specially designed for low resolution high altitude flight through multi-objective optimization can significantly improve overall aerodynamic performances of HAPS. This multidisciplinary approach also enables the enhancement of particular aerodynamic characteristics, such as lift gradient, maximal lift coefficient, minimal drag coefficient, behavior near stall, *etc.*
- Coupling different optimization and computational methods can result in streamlined geometries of significantly improved aerodynamic efficiencies and reduced power demands. Even though the obtained results should be taken with some reserve (particularly if simpler

computational models are employed), significantly greater flexibility in engineering design can be achieved and a large number of possible designs can be analyzed and compared in a relatively short amount of time.

- In order to increase the useful reference area (extremely important for solar panels), a multi-section wing with rectangular inner part should be employed, while the reduction of induced drag can be achieved by adopting high aspect-ratio wings. In order to diminish elastic deformations of extremely flexible wing structure, dihedral geometry should be adopted.
- In particular, here, HAPS weighing 150 kg will be able to cruise and glide at velocity 25 m/s and altitude 15-20 km, if it is equipped with a wing whose reference area is approximately 46.5 m^2. It is recommended to use a designed airfoil whose maximal relative thickness and curvature are 12.5% and 5%, respectively, located around the 1st third of the chord length.
- Although just a portion of solar energy can be converted to electricity, thin-film solar cells distributed along the upper surface of the wing (where at least 75% wing surface is used) can provide sufficient power for long endurance flight if their efficiency is 0.23-0.31. Their performance can be additionally improved by smart control strategies.

Acknowledgment

The research work is supported by the Ministry of Education, Science, and Technological Development of the Republic of Serbia through contract No. 451-03-9/2021-14/200105.

References

[1] D'Oliveira, F. A., *et al*., High-Altitude Platforms − Present Situation and Technology Trends, *Journal of Aerospace Technology and Management*, *8* (2016), 3, pp. 249-262
[2] Noth, A., Design of Solar Powered Airplanes for Continuous Flight, Ph. D. thesis, ETH Zurich, Zurich, Switzerland, 2008
[3] Alsahlani, A. A. M., Design of a Swept-Wing High-Altitude Long-Endurance Unmanned Air Vehicle (HALE UAV), Ph. D. thesis, University of Salford, Manchester, UK, 2017
[4] Colas, D. F., *et al*., The HALE Multidisciplinary Design Optimization – Part I: Solar-Powered Single and Multiple-Boom Aircraft, *Proceedings*, 18th AIAA Aviation Technology, Integration, and Operations Conference, Atlanta, Geo., USA, 2018
[5] Colas, D. F., *et al*., The HALE Multidisciplinary Design Optimization – Part II: Solar-Powered Single and Multiple-Boom Aircraft, *Proceedings*, 18th AIAA Aviation Technology, Integration, and Operations Conference, Atlanta, Geo., USA, 2018
[6] Gibbs, Y., *The NASA Armstrong Fact Sheet: Helios Prototype*, NASA, Edwards, Cal., USA, 2015
[7] ***, BAE Systems, https://www.baesystems.com/en/product/phasa-35
[8] Goraj, Z., Spalding, D., Design Challenges Associated with Development of a New Generation UAV, *Aircraft Engineering and Aerospace Technology*, *77* (2005), 5, pp. 361-368
[9] Park, K., *et al*., Optimal Design of Airfoil with High Aspect Ratio in Unmanned Aerial Vehicles, World Academy of Science, *Engineering and Technology*, *40* (2009), Apr., pp. 182-188
[10] Gardner, A. B., Selig, M. S., Airfoil Design Using a Genetic Algorithm and an Inverse Method, *Proceedings*, 41st Aerospace Sciences Meeting and Exhibit, Reno, Nev., USA, 2003, p. 12
[11] Leloudas, S. N., *et al.*, Airfoil Optimization Using Area-Preserving Free-Form Feformation, *Proceedings*, ASME International Mechanical Engineering Congress and Exposition, Houston, Tex., USA, 2015, Vol. 1, p. 10
[12] Mukesh, R., *et al.*, Airfoil Shape Optimization Using Non-Traditional Optimization Tecnique and Its Validation, *Journal of King Saud University − Engineering Sciences*, *26* (2014), 2, pp. 191-197
[13] Viola, I. M., *et al.*, Optimal Airfoil's Shapes by High Fidelity CFD, *Aircraft Engineering and Aerospace Technology*, *90* (2018), 6, pp. 1000-1011
[14] Qiu, L., *et al.*, Airfoil Profile Optimization of an Air Suction Equipment with an Air Duct, *Thermal Science*, *19* (2015), 4, pp. 1217-1222
[15] Natarajan, K., *et al.*, Numerical Investigation of Airfoils for Small Wind Turbine Applications, *Thermal Science*, *20* (2016), Suppl. 4, pp. S1091-S1098

[16] Ivanov, T. D., *et al.*, Influence of Selected Turbulence Model on the Optimization of a Class-Shape Transformation Parameterized Airfoil, *Thermal Science*, *21* (2017), Suppl. 3, pp. S737-S744
[17] Peigin, S., *et al.*, Unmanned Air Vehicle 3-D Wing Aerodynamical Design and Algorithm Stability with Respect to Initial Shape, *Thermal Science*, *23* (2019), Suppl. 2, pp. S599-S605
[18] Drela, M., *The XFOIL Formulation, Formulation of Computer Program XFOIL*, Massachusetts Institute of Technology, Cambridge, Mass., USA, 2008
[19] Langtry, R. B., Menter, F. R., Transition Modelling for General CFD Applications in Aeronautics, *Proceedings*, 43rd AIAA Aerospace Sciences Meeting and Exhibit – Meeting Papers, Reno, Nev., USA, 2005, pp. 15513-15526
[20] Kulfan, B. M., Bussoletti, J. E., "Fundamental" Parametric Geometry Representations for Aircraft Component Shapes, *Proceedings*, 11th AIAA/ISSMO Multidisciplinary Analysis and Optimization Conference, Portsmouth, Va., USA, 2006, Vol. 1, pp. 547-591
[21] Beasley, D., *et al.*, An Overview of Genetic Algorithms – Part 1: Fundamentals, *University Computing*, *15* (1993), 2, pp. 58-69
[22] Beasley, D., *et al.*, An Overview of Genetic Algorithms – Part 2: Research Topics, *University Computing*, *15* (1993), 4, pp. 170-181
[23] Selig, M., McGranahan, B., *Wind Tunnel Aerodynamic Tests of Six Airfoils for Use on Small Wind Turbines*, NREL/SR-500-34515, National Renewable Energy Laboratory, Golden, Col., USA, 2004
[24] ***, ANSYS Fluent Theory Guide, ANSYS, Inc., Canon-sburg, Pa., USA, 2017
[25] Hasan, M. S., *et a*l., Conceptual Design and Fluid Structure Interaction Analysis of a Solar Powered High-Altitude Pseudo-Satellite (HAPS) UAV Wing Model, *Proceedings*, (Lecture Notes in Mechanical Engineering), International Symposium for Production Research ISPR 2020, Antalya, Turkey, 2020, pp. 93-105
[26] Svorcan, J., *et al.*, Optimal Propeller Design for Future HALE UAV, *Scientific Technical Review*, *69* (2019), 2, pp. 25-31
[27] ***, Global Solar Atlas, https://globalsolaratlas.info/map
[28] Zubi, G., *et al.*, The Lithium-Ion Battery: State of the Art and Future Perspectives, *Renewable and Sustainable Energy Reviews*, *89* (2018), June, pp. 292-308

Paper submitted: April 19, 2021
Paper revised: June 27, 2021
Paper accepted: July 16, 2021